Applications in Energy and Combustion Science 14 (2023) 100122

Contents lists available at ScienceDirect

Applications in Energy and Combustion Science

journal homepage: www.sciencedirect.com/journal/applications-in-energy-and-combustion-science

Blowout dynamics and plasma-assisted stabilization of premixed swirl flames under fuel pulsations

Jinguo Sun [a], Hu Wu [a], Yong Tang [b], Chengdong Kong [c], Shuiqing Li [a,*]

[a] Key Laboratory for Thermal Science and Power Engineering of Ministry of Education, Department of Energy and Power Engineering, Tsinghua University, Beijing, 100084, China
[b] School of Aerospace Engineering, Beijing Institute of Technology, Beijing 100081, China
[c] Institute of Thermal Energy Engineering, Shanghai Jiao Tong University, Shanghai 200240, China

ARTICLE INFO

Keywords:
Fuel pulsation disturbance
Premixed swirl flame (PSF)
Lean blowout (LBO) limits
Microsecond repetitively pulsed (MRP) discharges
Discharge time delay

ABSTRACT

The present work investigates blowout dynamics of premixed swirl flames under low-frequency high-amplitude flow pulsations from the fuel feedline, and applies microsecond repetitively pulsed discharges with extremely-low power consumption to precisely control the stability of pulsating flames. First, both positive and negative fuel pulsations deteriorate the flame stability, causing much-narrowed lean blowout regimes. The fuel pulsation causes the flame to remain at the fuel-lean condition for a long period of time, which is considered to be the main cause of flame blowout. The flame response can be further explained by the convection process of the equivalence ratio oscillation. Secondly, the microsecond pulsed discharge with the same repetition rate as the fuel pulsation is used to alter the lean blowout via thermal, kinetic, and hydrodynamics effects. More importantly, the time delay between the discharge pulse and the fuel pulsation determines whether the plasma has an enhancement effect or not. It is found that the discharge prior to the convection of the equivalence ratio pulsation reaches the optimal effectiveness for flame stabilization, extending the blowout limit by approximately 10%. Finally, the lean blowout limit can be continuously extended with the increasing discharge repetition rate until saturation.

1. Introduction

In the development of advanced gas turbines and aero-engines designed for low NO_x emission and high-power outputs, the prediction and control of flame extinction (referred to here as lean blowout, LBO) are of great significance [1–4]. It is necessary to comprehensively understand the blowout dynamics, especially under various kinds of disturbances [5–8]. Such disturbance can be harmonic, impulsive, and their superposition that contains multiple frequencies from several hertz to kilohertz [9]. The flame blowout characteristics under harmonic disturbances were systematically investigated in numerous studies [5,6]. Yet, less attention was paid to the blowout dynamics under low-frequency impulsive disturbances that naturally arise under transient operating conditions like chock, chugging, or surge of most combustors [7].

Under lean conditions, disturbances of the inflowing air, fuel, or their mixture cause fluctuations of inlet velocity and equivalence ratio, subsequently triggering heat release rate oscillations and then flame blowout [8]. Recently, we employed a low-frequency, high-amplitude flow pulsation on the air feedline to disturb the swirl flame, resulting in significant disturbances in both inlet velocity and equivalence ratio. It was found that the flame stability became worse mainly due to the breakdown of the flame front caused by flow separation [10,11]. When the fuel flow was harmonically disturbed, lean blowout issues were mainly attributed to the equivalence ratio perturbation [8]. For sinusoidal disturbance of inlet equivalence ratio with a frequency of 100-400 Hz, lean blowout occurred at strong oscillations of equivalence ratio, and the flame response can be divided into linear and nonlinear regimes depending on the oscillation amplitude [8]. However, the combustion failure issue caused by low-frequency impulsive fuel pulsation was rarely reported. Therefore, this work integrates a flow pulsating system into the fuel feedline of a premixed swirl flame (PSF) to produce low-frequency impulsive fuel flow disturbances, and the first purpose is to study the blowout dynamics under such inlet fuel pulsations.

The control strategy for flame blowout issues has been explored for more than a century. Several passive/active control techniques, such as fuel flow redistribution [12], secondary fuel injection [13], and addition

* Corresponding author.
E-mail address: lishuiqing@tsinghua.edu.cn (S. Li).

https://doi.org/10.1016/j.jaecs.2023.100122
Received 29 November 2022; Received in revised form 20 January 2023; Accepted 16 February 2023
Available online 24 February 2023

Nomenclature

$a_i(t)$	time coefficient of i^{th} POD mode
d_c	diameter of the center body, m
d_n	diameter of the nozzle, m
f	repetition rate of the pulsed discharge, Hz
I	current, A
L	distance, m
P_{dis}	discharge power, W
Q_{air}	air flow rate, L/min
r	radial location in cylindrical coordinate, m
St_d	Strouhal number of the discharge
S_{OH}	frame-integrated OH-PLIF signal intensity
Sw	swirl number
t	time, s
u	flow velocity of gas flow, m/s
V	voltage, V
z	axial location in cylindrical coordinate, m
α	inclined angle of the swirler, °
ϕ	equivalence ratio
λ_i	energy content or eigenvalue of i^{th} POD mode
$\varphi_i(x)$	empirical orthogonal function of i^{th} POD mode
τ_{dis}	time delay between the flow pulsation and the discharge pulse, s
τ_{conv}	convective time of the equivalence ratio fluctuation, s

Subscripts

dis	discharge
in	inlet
LBO	lean blowout

of hydrogen [14] were developed to prevent LBO. However, more fast and efficient control methods are still urgently needed. In the recent decade, the novel plasma discharge has attracted much attention for its fast response and wide range of actuating frequency [15–17]. Such plasmas include plasma jet/torch [18], dielectric barrier discharge [19], microwave discharge [20–23], gliding arc discharge [24–32], and nanosecond/microsecond repetitively pulsed (NRP/MRP) discharge [10,11,33-39], etc. The non-equilibrium NRP discharge consuming much less energy than the thermal power of flame was frequently used to extend the static stability domain [38,39]. In addition, it can mitigate combustion instabilities under harmonic disturbances of the inlet flow [40], but may have the opposite effect when the discharge and acoustics at the resonance frequency are in phase [41]. More recently, we applied a low-repetition-rate MRP discharge to stabilize unsteady flames under impulsive disturbances from air flow. The MRP discharge improved the flame stability only at some specific time delays between pulses of air flow and discharge [10,11]. Yet, concerning the pulsating disturbance from the fuel feedline, how the MRP discharge affects the blowout dynamics is critical to overcoming the fuel pulsation issues but remains unrevealed. Therefore, this work attempts to use the non-equilibrium MRP discharge to address the potential issue of combustion deterioration caused by fuel flow pulsations.

The paper is organized as follows. Section 2 details the experimental methodology, including premixed swirl burner, specially-designed fuel pulsation actuator, microsecond repetitively pulsed discharge, and OH planar laser-induced fluorescence (OH-PLIF) measurement system. In Section 3, we first present lean blowout (LBO) limits at different kinds of fuel pulsations and flow rates. Then, more insights into the flame response to fuel pulsation, especially blowout dynamics, are obtained from the phase-locked OH-PLIF measurement. Finally, the effect of

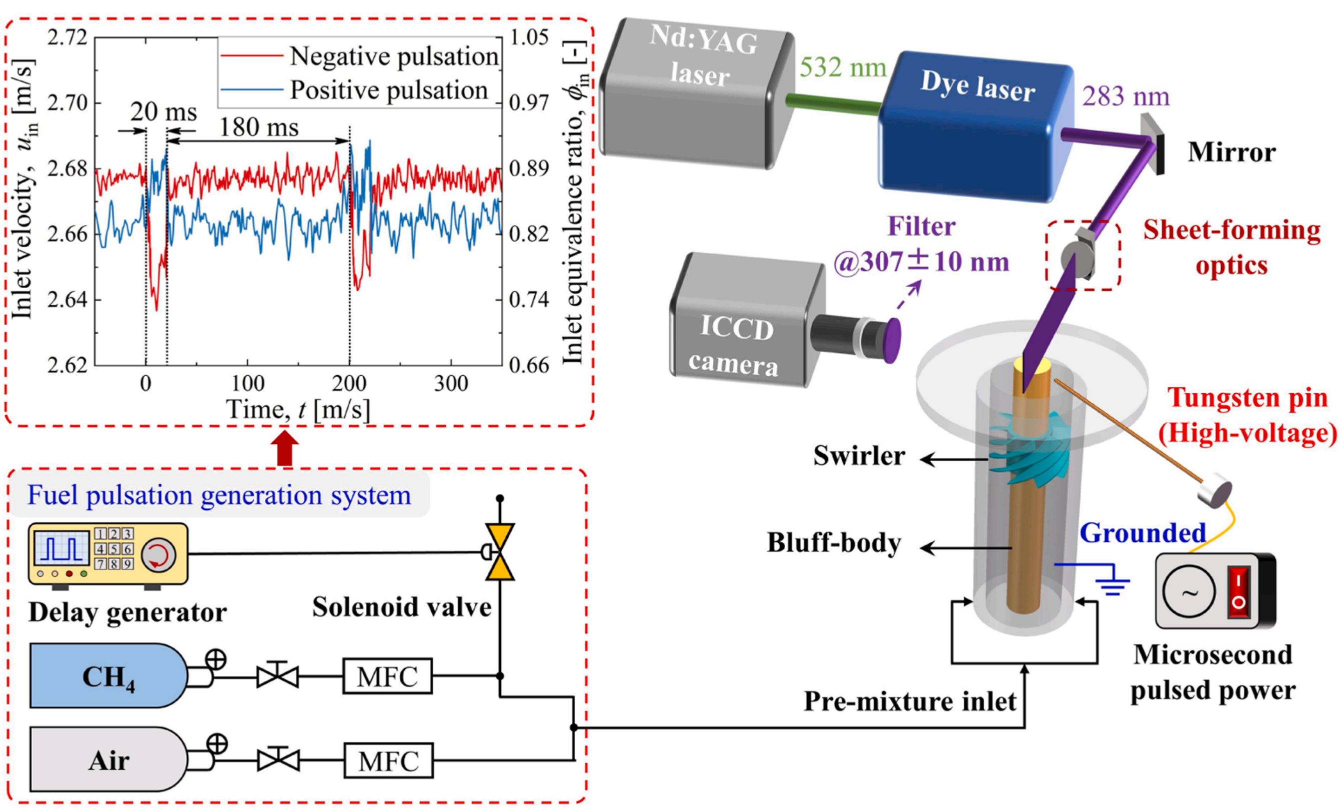

Fig. 1. A schematic of the experimental setup including the premixed swirl burner, fuel pulsation actuator, MRP discharge, and OH-PLIF measurement system.

microsecond pulsed discharge on pulsating flame stability is demonstrated. The underlying mechanism of plasma-assisted stabilization under fuel pulsation is quantitatively unraveled by the proper orthogonal decomposition (POD).

2. Experimental methodology

2.1. Premixed swirl burner

Fig. 1 shows a schematic of the experimental setup including the premixed swirl burner, the fuel pulsation generation system, the microsecond repetitively pulsed discharge system, and the OH planar laser-induced fluorescence system. This burner consists of a nozzle with an inner diameter of 18 mm, a cylindrical center body with a diameter of 8 mm, and a vane swirler installed on the center body. The methane and air inflows are well premixed in a mixing chamber before entering the burner. And then, the pre-mixture passes through the swirler, forming a swirling flow. Here, the swirl number of 0.75 is determined from the following formula [42]:

$$Sw = \frac{2}{3}\tan(\alpha)\frac{1-(d_c/d_n)^3}{1-(d_c/d_n)^2} \tag{1}$$

where $\alpha = 45^\circ$ denotes the inclined angle of the swirler, d_c and d_n are the diameters of the center body and nozzle, respectively.

2.2. Fuel flow pulsations

Low-frequency, high-amplitude pulsations in the fuel feed line are generated by a fast-acting solenoid valve (MAC35A-ACA). The valve is connected to the bypass pipe and regulated by a quasi-rectangular signal from a digital pulse generator (Stanford Research Systems, Model DG645, $<$ 25 ps rms jitter) to control the open duration and the repetition rate. All fuel flows into the burner only when the valve is closed. And when the valve is open, approximately 15% of the fuel is emitted to the ambient through the bypass. The repetition rate is set to 5 Hz, much lower than the cut-off frequency of the flame as a low-pass filter [43]. By varying the valve-open duration, two kinds of pulsations are formed, which are named the positive pulsation and the negative pulsation, respectively. For the positive pulsation, the valve opens for 180 ms within one cycle and closes for the remaining 20 ms, causing the flow rate of fuel to increase as a positive pulse. For the negative pulsation, the valve opens for 20 ms and closes for 180 ms, inducing a negative pulse of the fuel flow. The flow rates under these two pulsations are the same. The rise and fall times of each flow pulse are around 2 ms.

In the condition of cold flows without flames, the time-varying velocity of the non-reacting jet flow at the burner exit is measured by using Laser Doppler Velocimetry (LDV) to characterize the velocity fluctuations under flow pulsation. The inset of Fig. 1 shows the typical waveforms of pulsating inlet velocity (u_{in}) at an air flow rate (Q_{air}) of 30 L/min, which appear in quasi-rectangular shapes. The right coordinate denotes the corresponding inlet equivalence ratio (ϕ_{in}) calculated based on a constant Q_{air}, and the fluctuation of ϕ_{in} exceeds 10%. Unlike the air flow pulsation which caused the inlet velocity fluctuation of over 10% [10,11], herein, the relative fluctuation of mean flow velocity is only 1.5%, inducing much less influence on the flow field than that on the equivalence ratio.

2.3. Microsecond repetitively pulsed discharge

A 1-mm-diameter tungsten pin connected to a homemade microsecond pulsed power supply (CMPC-40D) is placed near the nozzle exit to serve as a high-voltage electrode, while the stainless-steel center body is grounded. The burner nozzle is insulated by a quartz plate fixed on it. Through preliminary tests, the gap distance between the pin tip and the center rod is set to 6 mm as an optimal arrangement, ensuring a large discharge volume with a moderate breakdown voltage. Direct photographs of the MRP-spark discharges in the air and flames ($\phi = 0.85$, $Q_{air} = 30$ L/min) are shown in the insets of Fig. 2. The high-voltage electrode located in the flame region interacts with the bluff body to generate a plasma discharge. The discharge column with a length of around 6 mm and a diameter of around 1 mm spans across the flame zone and inner recirculation zone so that it can process the combustible pre-mixture well. The repetition rates of the MRP discharge and the flow pulsation can be independently adjusted, thus to study the interactions between discharge pulse and pulsating flame flexibly.

The voltage (V) and current (I) are measured by a high-voltage probe (Tektronix P6015A, 75 MHz) and a current monitor (Pearson 4100, 35 MHz), respectively, and are simultaneously recorded by an oscilloscope (Tektronix DPO2024B, 200 MHz). The peak voltage and current are 9.2 kV and 28.6 A, respectively. The rise time and the width of the high-voltage pulse are approximately 0.5 μs and 8 μs [44]. Typically, after gas breakdown, the voltage falls to zero within a few nanoseconds and then oscillates, and the current decays in the form of sinusoidal oscillation within about 40 μs. The discharge energy deposition increases rapidly in the first 0.5 μs, and then reaches a plateau until 40 μs. The total energy deposition of each pulse is approximately 9.0 mJ, corresponding to an average discharge power of only 45 mW at a repetition rate of 5 Hz. The discharge power does not exceed 0.1% of the thermal power of 1.51 kW at $Q_{air} = 30$ L/min and $\phi = 0.8$, provided that the fuel is completely consumed.

2.4. Phase-locked OH-PLIF measurement

The OH-PLIF system is illustrated in Fig. 1. A frequency-doubled dye laser (Sirah Cobra-Stretch) is pumped by an Nd:YAG laser (Quanta Ray LAB-170) at a frequency of 5 Hz to produce a laser beam of 283 nm at 6 mJ/pulse. The laser beam is expanded into a 0.5-mm-thick laser sheet by sheet-forming optics and then is introduced perpendicularly to illuminate the central slice of the swirl flame. An ICCD camera (Princeton PIMAX-IV, 1024 $\times$ 1024 pixels) equipped with a 307±10 nm filter collects the OH fluorescence with a gate width of 100 ns. When the discharge is activated, the exposure time adopted is short enough to reduce the spontaneous emission of the MRP-spark discharge and capture the relatively pure ground-state OH PLIF signal. For each case, 100 single-shot images are recorded over a field of view of 60 $\times$ 60 mm^2, yielding a spatial resolution of 0.059 mm/pixel. The laser pulse, the discharge pulse, and the flow pulse are synchronized using the digital pulse generator DG645 to measure the phase-locked OH distributions during the forcing period.

3. Results and discussion

3.1. LBO limits of perturbed flames without MRP discharges

At ambient temperature (298 K) and atmospheric pressure (1 atm), the flame is first ignited and maintained for at least 5 minutes to ensure the thermal steady state. By slowly reducing the equivalence ratio until the flame blowout, LBO limits of PSFs without and with negative/positive fuel pulsations are obtained and depicted in Fig. 3. Here, the lean blowout equivalence ratio (ϕ_{LBO}) is calculated based on the time-averaged fuel flow rates in one period of pulsation. For example, in a negative pulsation case with a time-averaged ϕ_{in} of 1.01, the instantaneous ϕ_{in} during 0-20 ms is approximately 0.87, and the lean flame will be blown off. The measurement uncertainty is within 5%, which is derived from the standard deviations of at least three repetitive measurements and the accuracy of flow meters. For perturbed cases, we specifically set a very low regulation rate of fuel that reduces the equivalence ratio by about 0.06 per min, much slower than the fuel flow pulse with the 2-ms rise and fall times. The insets of Fig. 3 also show the direct photography of typical “attached” and “detached” axisymmetric V-shaped swirl flames. Under the periodic perturbation of the fuel

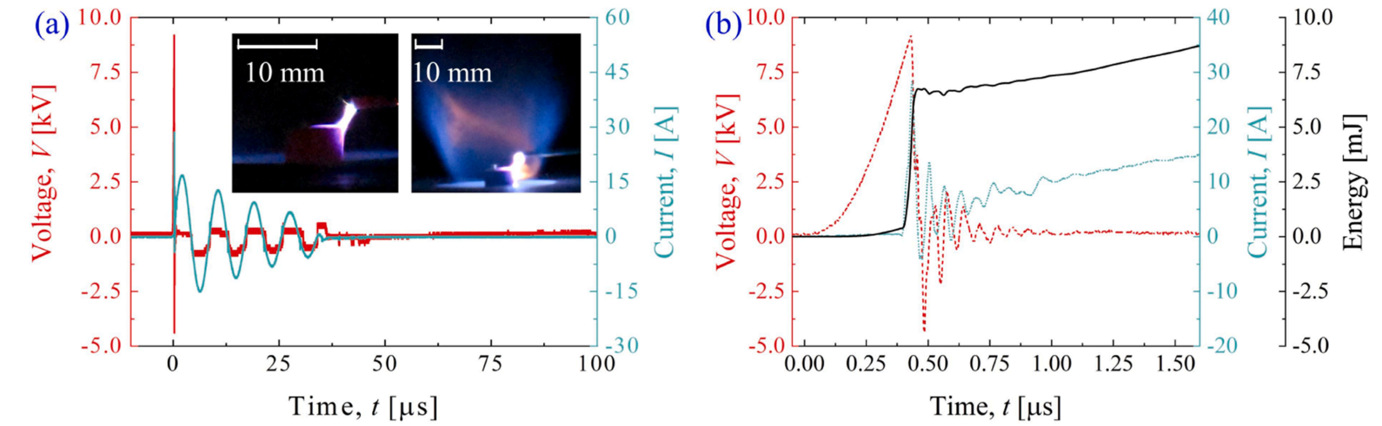

Fig. 2. (a) Typical waveforms of the voltage and current of the microsecond repetitively pulsed discharge within 100 µs, (b) a zoomed-in view within 1.75 µs, including the integrated energy deposition.

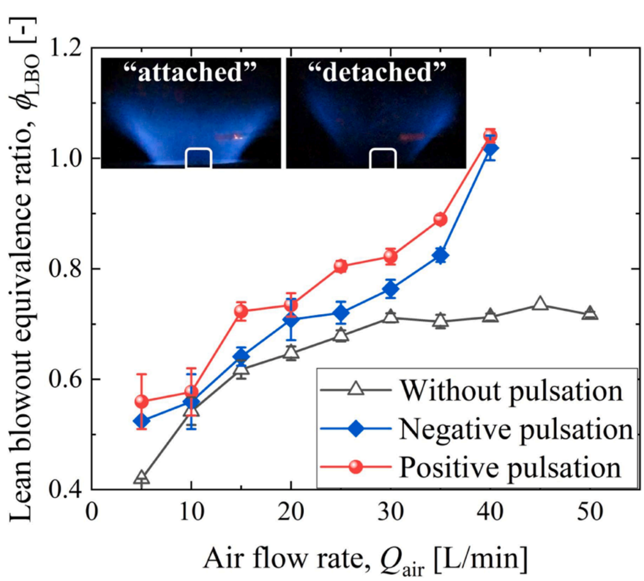

Fig. 3. LBO limits of PSFs under negative and positive fuel flow pulsations and non-perturbed conditions. The insets denote the images of the flame ($\phi = 0.85$, $Q_{air} = 30$ L/min) taken by the Nikon camera with an exposure time of 1/60 s.

pulsation, the flame attaches to and detaches from the center body repetitively, resulting in an unstable combustion mode and even blowout.

As indicated in Fig. 3, ϕ_{LBO} increases rapidly with Q_{air}. As Q_{air} is adjusted from 5 L/min to 40 L/min, ϕ_{LBO} increases from 0.42 to 0.72 for the non-perturbed conditions but increases from 0.53 to 1.02, and from 0.56 to 1.04 for negative and positive pulsations, respectively. In particular, at a flow rate of 40 L/min, the unperturbed flame can be stabilized with an equivalence ratio of 0.71, whereas ϕ_{LBO} of the perturbed flame exceeds 1.0, exhibiting a remarkable increment (up to 46%). It thus confirms that the lean flames are prone to blow out under the disturbance of fuel flow pulsation.

Moreover, the combustion deterioration under positive fuel pulsations is more severe compared to that under negative fuel pulsations. The equivalence ratio curves in Fig. 1 indicate that, at the same time-averaged inlet equivalence ratio of 0.85 and flow rate, the instantaneous ϕ_{in} under negative fuel pulsation is higher than that under positive fuel pulsation within a long duration (180 ms). Therefore, the flame perturbed by the positive fuel pulsation is more susceptible to being extinguished, resulting in a higher ϕ_{LBO}. The following sections mainly focus on the cases of positive fuel pulsations.

3.2. Flame blowout dynamics under positive fuel pulsations

The phase-locked OH-PLIF techniques have been utilized to visualize the premixed flame dynamics under positive fuel pulsations. Fig. 4 shows a sequence of instantaneous OH-PLIF images covering a complete disturbance cycle (0-190 ms, with an interval of 10 ms). The insets of Fig. 5 display the instantaneous OH-PLIF images of the perturbed PSFs at different time delays after the triggering of flow pulsation. The laser sheet propagates from left to right and is partially blocked by the center body, causing blanks on the right bottom side of OH-PLIF images. Here, the axisymmetric OH radical distribution identifies the typical V-shaped flame stabilized on the bluff body.

With background subtraction and laser sheet correction, the frame-integrated OH-PLIF signal intensity (S_{OH}) is calculated to indicate the temporal combustion intensity of the pulsating combustion process [45], as shown in Fig. 5. The data points and the error bars represent the averages and standard deviations of 100 snapshots, respectively. The evolution of S_{OH} indicates three distinctive combustion stages as follows: (a) it decreases during 0-40 ms and reaches a plateau thereafter till 90 ms, (b) then it elevates during 90-130 ms and reaches another plateau till 160 ms, (c) eventually it drops to the original state until the next cycle.

During stage (i), the V-shaped flame is slightly weakened and then maintained, as indicated by the inset snapshots at $t = 10$ ms and 50 ms in Fig. 5. After 90 ms, a transition representing intensified combustion occurs during stage (ii). The snapshot at 120 ms shows that the reaction zone is expanded with an increased flame opening angle (from 25° to 43°), which implies a broadened inner recirculation zone (IRZ) along the centerline. The IRZ with low/reversed velocities can provide a more favorable environment for the fresh reactants to be continuously ignited by the recirculated hot products. However, beyond stage (ii), a weakened flame is exhibited according to the OH-PLIF results, which lasts until the next disturbance cycle.

According to the observations of the near-limit flames, the blowout mostly occurs over the periods of 0-90 ms and 160-200 ms, which is coincident with the frame-integrated OH-PLIF intensity analysis. In addition, the S_{OH} of flame under fuel pulsation always decreases to a value ($S_{OH} = 5 \times 10^7$), much lower than that of the unperturbed flame ($S_{OH} = 8 \times 10^7$). It means that the flame is significantly deteriorated due to the fuel pulsation, eventually causing a narrowed LBO limit.

To understand the aforementioned staged flame evolution, we here consider the transport of the positive fuel pulsation produced from the valve, which is inspired by the concept of convection delay in previous studies on harmonic disturbances [46]. The intensified combustion during stage (ii) is due to the temporally increased fuel supply, in other words, the inlet equivalence ratio. The distance between the valve and the flame front (L) results in a convective time delay (τ_{conv}),

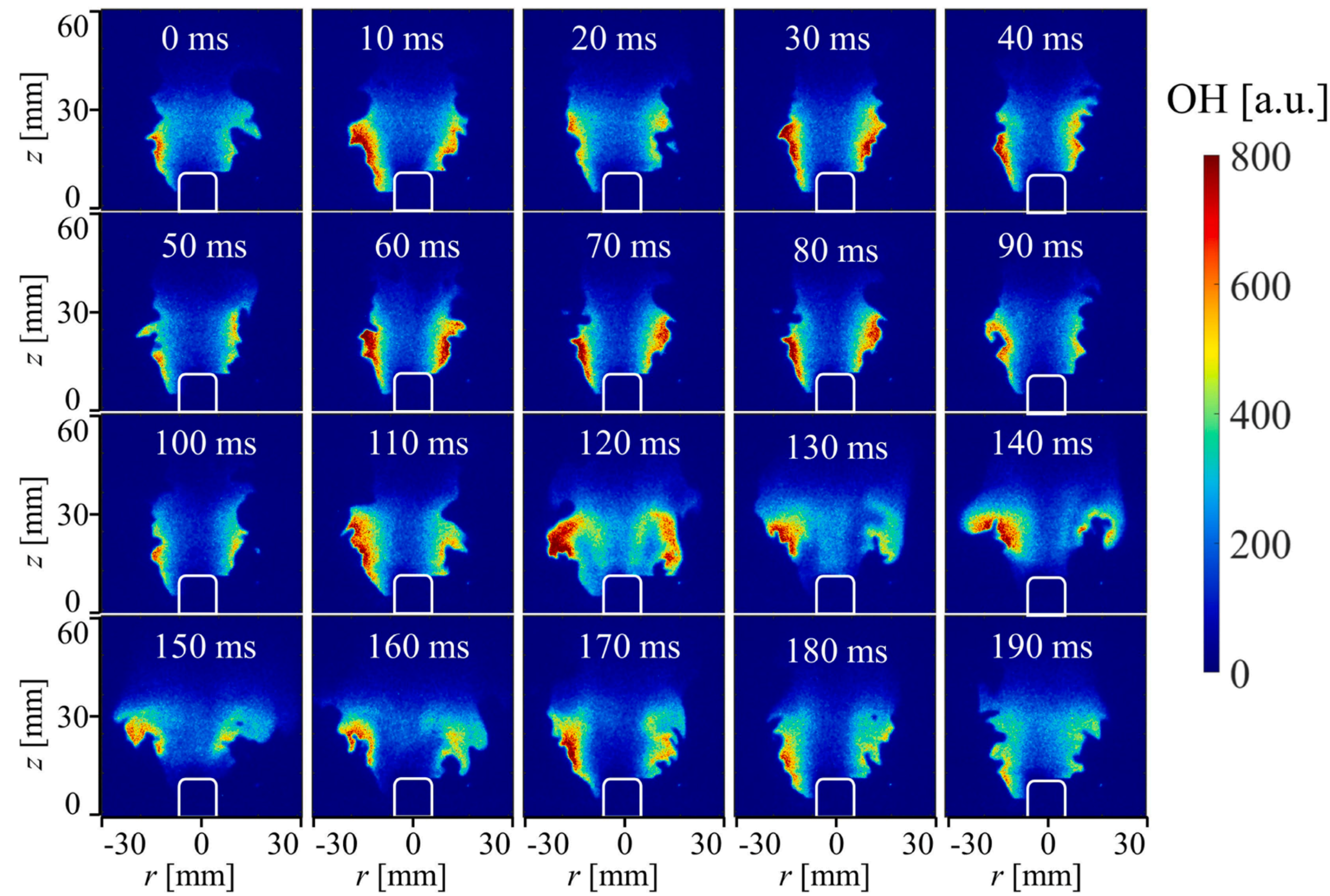

Fig. 4. Single-shot OH-PLIF imaging sequences of flames without the MRP discharge in one disturbance cycle.

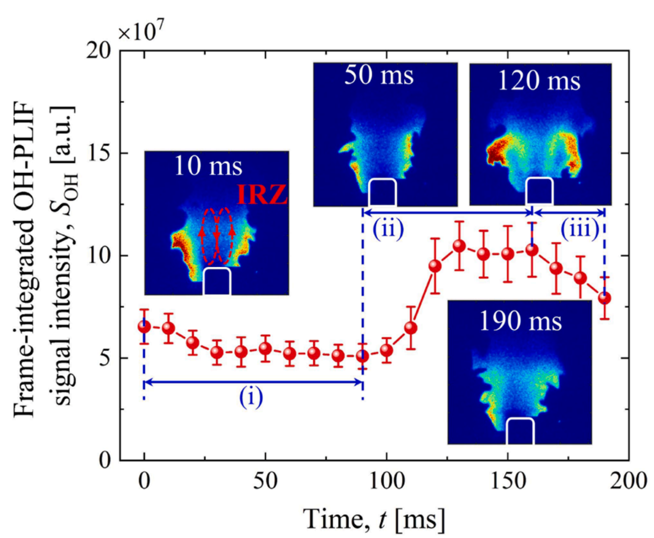

Fig. 5. Temporal variation of the frame-integrated OH-PLIF signal intensity with time under positive fuel pulsation. The recording time is marked in each inset graph.

$$\tau_{\mathrm{conv}} = \int_0^L 1 / u \,\mathrm{d}l \tag{2}$$

where u denotes the flow velocity [46,47]. Here, τ_{conv} is estimated to be 82.6 ms at Q_{air} = 30 L/min. Hence, it takes 82.6 ms for the flame to perceive the increased equivalence ratio caused by the positive fuel pulsation. The transition point of the S_{OH} curve around 90 ms is roughly coincident with the convective time delay, verifying that the flame evolution is dominated by the equivalence ratio fluctuation. It is frequently claimed that the equivalence ratio oscillation induced by pressure oscillations in the combustion chamber and then convected downstream is an intrinsic mechanism driving dynamic combustion instability. In particular, there is also a delay between the subsequent heat release and the equivalent ratio oscillation at the injector [46,48]. Thus, it can be argued that the convective delay of equivalence ratio always plays an essential role in both the mechanisms of dynamic and static combustion instability (referring to flame blowout). More importantly, the primary difference between them is the inducement of the equivalence ratio fluctuation. The former is caused by the pressure oscillation inside the combustor, whilst the latter is caused by the forcing pulsation of fuel intake.

Moreover, as seen in Fig. 1, the fuel flow pulsation is a quasi-rectangular waveform with sharp rising and falling edges. When such inflow perturbation convects downstream to the reaction zone, the rectangular pulse of equivalence ratio is expected to be flattened due to species diffusion driven by the sharp concentration gradient. Therefore, the S_{OH} curve in Fig. 5 has a flatter profile, suggesting a non-quasi-steady flame response. The non-quasi-steadiness was also found in the previous study of laminar stagnation flame perturbed by the quasi-rectangular air flow inlet pulsation, where the local stretch rate exhibited a flatter profile [49].

3.3. Active control of flame stability using MRP discharges

The 5 Hz MRP discharge is applied to actively stabilize the lean PSF with fuel flow pulsation. Here, the discharge time delay (τ_{dis}) between the MRP discharge and the fuel pulsation is defined and illustrated in the inset of Fig. 6, and its influence on the LBO limit is thus explored. A horizontal dashed line ($\phi_{LBO} = 0.82$), representing the lean blowout equivalence ratio of flame at $Q_{air} = 30$ L/min and without the MRP discharge, is plotted to assess the effect of the discharges on flame stabilization. Accordingly, two regimes with and without stability enhancement are distinguished. In the enhancement regime, when τ_{dis} is in the range of 0-80 ms and 160-200 ms, ϕ_{LBO} is lower than 0.82, pronouncing the improved flame stability by the plasma. Particularly, for cases at $\tau_{dis} = 10$ ms, the LBO limit can be extended up to around 10% even though the discharge power is less than 0.1% of the thermal power. While in the non-enhancement regime, when the discharge is triggered between 80 and 160 ms, flame stability is not improved, and even blowout events become more prone to occur.

To elucidate the effects of the MRP discharges on perturbed flames in the two distinct regimes, the sequential OH-PLIF images of plasma-assisted flames under different conditions of $\tau_{dis} = 30$ ms (case A) and 130 ms (case B) are presented in Fig. 7, and the corresponding spatial-integrated OH-PLIF signal intensities are plotted in Fig. 8. The overall trends of these three curves are similar, as described in Section 3.2, but importantly, it can be distinguished that when the discharge is triggered at 30 ms, the OH-PLIF signal intensity is enhanced compared to that without plasma, especially at the flame root. In the repetitively pulsed discharge, more active radicals such as OH, H, and O can be produced through electron impact dissociation (e.g. $e + O_2 \rightarrow e + O + O(^1D)$) to constitute the radical pools, which play a vital role in chain-branching reactions [15,40,50,51]. Besides, this discharge channel with an energy deposition of 9.0 mJ/pulse, which is a kind of spark discharge to some extent [52], was proved to provide sufficient heat to ignite the fresh reactants [10,11]. Consequently, a combination of the plasma-induced active radicals and the addition of the discharge energy promotes the reignition process of the locally extinguished flame, stabilizing the near-limit flame. The extinction-reignition of perturbed flames with MRP discharges can be found in Supplementary Video S1.

As described in Section 3.2, the flame naturally experiences a periodic evolution due to the fuel pulsation. For case A, at $t = 30$ ms, when the flame is suffering from a reduced equivalence ratio and approaches blowout, the activated discharge prevents the flame from blowout, so that the flame can be sustained until the subsequent stage (ii). In this manner, the LBO limit is extended. Note that the flame in stage (i) is inherently weaker and has a higher risk of a blowout than that in stage (ii) due to the lower local equivalence ratio, so the LBO limit of the perturbed flame depends more on stage (i) than on stage (ii). For case B, when the plasma is turned on at 130 ms, the flame in stage (ii) is reinforced. However, the enhancement effect of plasma on flame obviously cannot be sustained to stage (i) of the next disturbance cycle. Hence, the discharge makes little difference in the extension of the LBO limit. It can be concluded that the distinction between the regimes is closely related to the aforementioned three stages of perturbed PSFs (see Fig. 5).

Given the underlying connection between the convective time delay and the flame response, the regimes of LBO limits with MRP assistance can also be described in terms of the convective time delay. Specifically, to overcome the detrimental effects of the pulsating disturbance on combustion, the discharge time delay should be smaller than the convective time delay, so that the plasma-induced reignition and enhancement can take crucial effects at the leaner equivalence ratio stage. In addition, the convective time delay of a flow system is readily available from the injector and operational designs, thus it is of practical significance to evaluate the optimal discharge time delay.

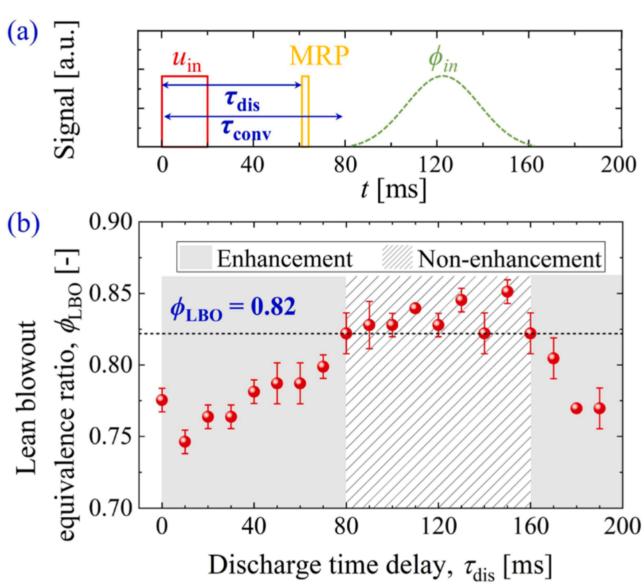

Fig. 6. (a) A schematic of the discharge time delay and the convective time delay, and (b) LBO limits of PSFs under positive fuel pulsations with various discharge time delays.

3.4. Proper orthogonal decomposition on plasma-assisted flame dynamics

Proper orthogonal decomposition is employed on the OH-PLIF imaging sequences to eliminate the redundancies in the dataset and reduce them into a lower-dimension linear subspace. Thus, it enables us to quantitatively extract coherent structures of a multi-scale chaotic system, in this study, swirl flames where fuel pulsation and pulsed discharge coexist. A time-dependent scalar field $Q(x, t)$ can be decomposed into a set of orthogonal functions, as follows [53]:

$$Q(x,t) = a_0(t)\varphi_0(x) + \sum_{i=1}^{i=N-1} a_i(t)\varphi_i(x) \tag{3}$$

$$\langle Q(x,\ t) \bullet Q^T(x,\ t)\rangle \varphi_i(x) = \lambda_i \varphi_i(x) \tag{4}$$

where N is the number of frames in the given dataset, the subscript i is the model index, the superscript T is the transpose operator and $\bullet$ the ensemble averaging operator, $\varphi_i(x)$, $a_i(t)$, and λ_i denote the empirical orthogonal functions, time coefficient, and eigenvalue of i^{th} POD mode, respectively. The modes are ordered according to the eigenvalue λ_i, which describes the energy content in descending order ($\lambda_i > \lambda_{i+1}$). Particularly, the first POD mode $\varphi_0(x)$ and eigenvalue λ_0 can be used to represent the ensemble-averaged structure and the mean energy content, respectively. Subsequent POD modes represent turbulent structures.

When computing the enormous autocorrelation matrix for a large number of grids, the computational memory is always a limitation. Hence, we adopt the method of snapshots proposed by Sirovich [54] to obtain the POD modes. Detailed mathematical procedures are available in the literature [54,55]. At each phase in the disturbance cycle (from 0 ms to 190 ms, with an interval of 10 ms), 100 OH-PLIF snapshots are processed to achieve a phase-dependent POD, which essentially gives a set of modes to fully describe the primary features of OH distribution at that phase [56]. The convergence has been validated by comparing the POD outcomes derived from different ensemble sets of 50, 100, and 200 snapshots.

Fig. 9 shows the first three predominant POD modes at key instants of the above three cases. As the energy contents of the rest modes are less than 0.10 of the total energy, the first three POD modes are sufficient as representative modes for flame dynamics. For the perturbed flame without discharge, the axisymmetric mean field (mode 0) at $t = 30$ ms, which occupies 78% of the total energy, is distinguished from the turbulent ones. Subsequent modes 1 and 2 present counter vortex pairs rotating adjacent to the mean field, which was also observed in similar premixed swirl flames in our previous study [28]. Fig. 10 shows the mean energy contents of perturbed flames under three different discharge conditions (without discharge, $\tau_{dis} = 30$ ms, and $\tau_{dis} = 130$

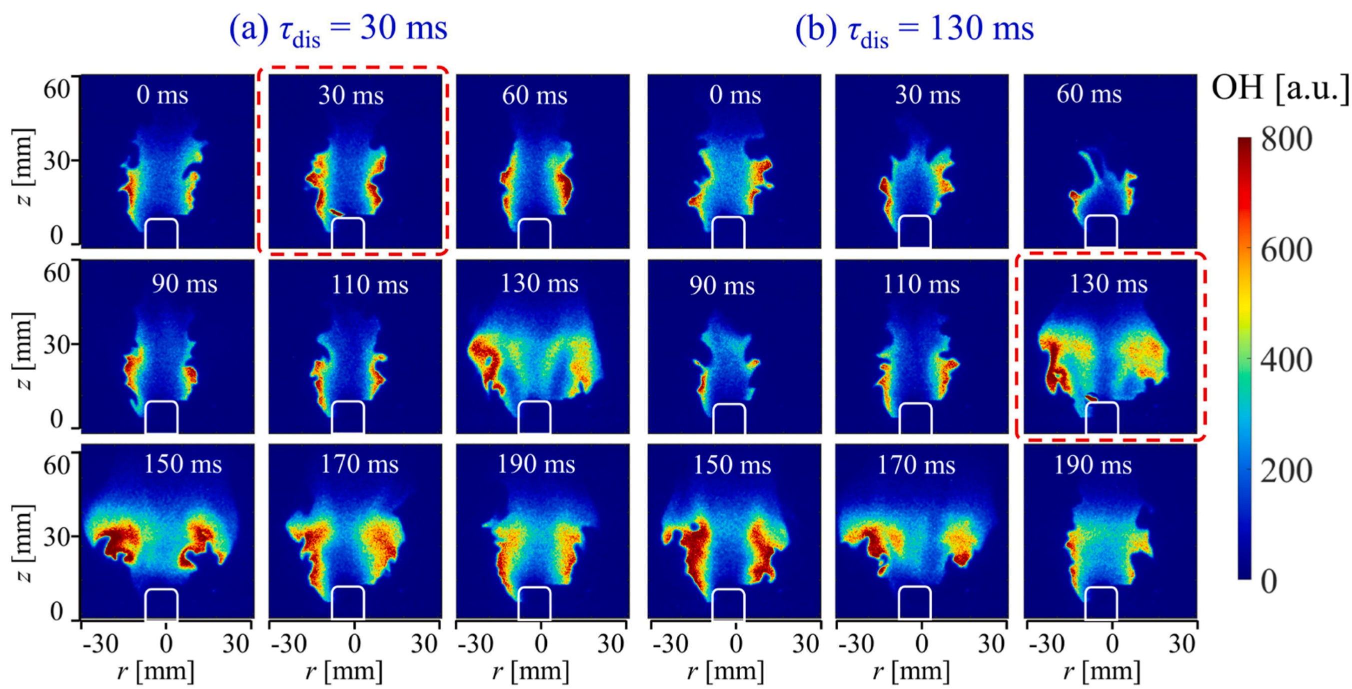

Fig. 7. Single-shot OH-PLIF imaging sequences of the premixed swirl flame perturbed by positive fuel pulsations, with different discharge time delays of (a) $\tau_{dis} = 30$ ms and (b) $\tau_{dis} = 130$ ms. The recording time is marked in each inset graph.

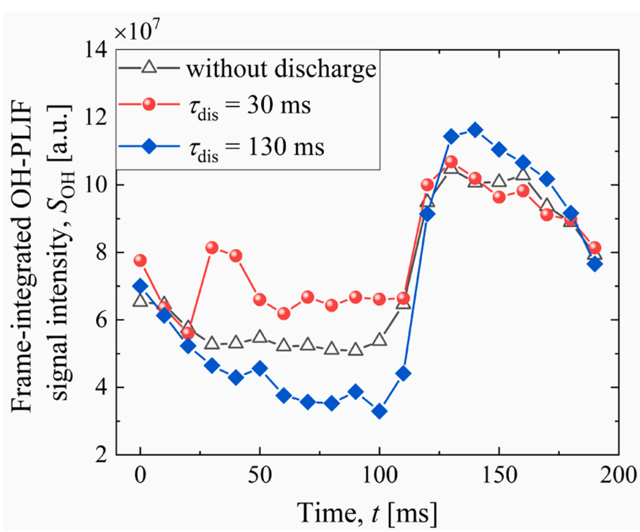

Fig. 8. Temporal variation of the frame-integrated OH-PLIF signal under fuel flow pulsation.

ms). In the absence of the MRP discharge, the curve of λ_0 ranges from 0.77 to 0.86. Fuel pulsation redistributes energy between modes, resulting in a temporal change in λ_0. The persistently high value of λ_0 and mode 0 in Fig. 9 indicates that the primary structure is not destroyed but merely suppressed by the fuel pulsation. There are some featured transitions in the temporal evolution. At around t = 100-120 ms, λ_0 slightly increases and then decreases until $t = 160$ ms. Apparently, these transition points are consistent with those of the S_{OH} curve, as observed in Fig. 8.

The mean energy content is modified when applying the MRP discharge. For the case of $\tau_{dis} = 30$ ms, the curve of λ_0 in the whole disturbance period is overall shifted higher compared to that of flames without discharge. For example, λ_0 increases from 0.80 to 0.84 at t = 0 ms and from 0.78 to 0.85 at $t = 150$ ms, thereby the turbulent energy content correspondingly decreases by 4-7%. It is a good manifestation of the plasma-altered flame dynamics, where stable large-scale structures become more prevalent and small turbulence are suppressed, eventually resulting in improved flame stability [21,28]. More importantly, since the discharge power addition is less than 0.1% of the thermal power whereas the increment of the mean energy content is 4-7%, the improved flame stability should be mainly attributed to the overall altered swirl flame dynamics rather than simple energy superposition. The observations that small addition of discharge energy can lead to a much higher increment in mean energy content were also reported in other types of plasmas. For example, the microwave plasma discharge at less than 5% of the thermal power was found to significantly increase the mean energy content of swirl flames by about 23% [21]. Besides, we previously applied a gliding arc with discharge power equal to 3% of the thermal power to stabilize the flame under the air flow pulsation, and observed a much higher increment of 30% in mean energy content and decrement in turbulence content [28]. Generally speaking, the nonlinear effect of discharge on flame dynamics, especially the non-proportional change in energy content, can be attributed to the thermal and kinetic additions. When a small amount of discharge energy and active radicals are added, the almost quenching combustion reactions can be reactivated not only due to the strong nonlinear Arrhenius exponential relationship but also the chain branching processes of the radical pools. However, the discharge does not take effect on the quenching status in the case of $\tau_{dis} = 130$ ms. λ_0 is 5% lower than that of flame without discharge at t = 0-100 ms until the pulsed discharge is triggered, i.e., the MRP discharge shows little favoring for flame stabilization under fuel pulsation.

Moreover, the energy distribution significantly changes at the onset of the MRP discharge. As depicted in the second ($t = 30$ ms) and third rows ($t = 130$ ms) of Fig. 9, the counter-rotating vortex pairs in modes 1 and 2 disappear and are replaced by the surrounding turbulence. The energy content of modes 1 (λ_1) increases from 0.014 to 0.10 for $\tau_{dis} = 30$ ms and to 0.09 for $\tau_{dis} = 130$ ms, and the energy content of modes 2 (λ_2) increases from 0.013 to 0.09 for $\tau_{dis} = 30$ ms and to 0.05 for $\tau_{dis} = 130$ ms. It also can be seen from Fig. 10 that for $\tau_{dis} = 30$ ms, λ_0 significantly decreases from 0.81 to 0.61 at $t = 30$ ms. Similarly, in the case of $\tau_{dis} =$

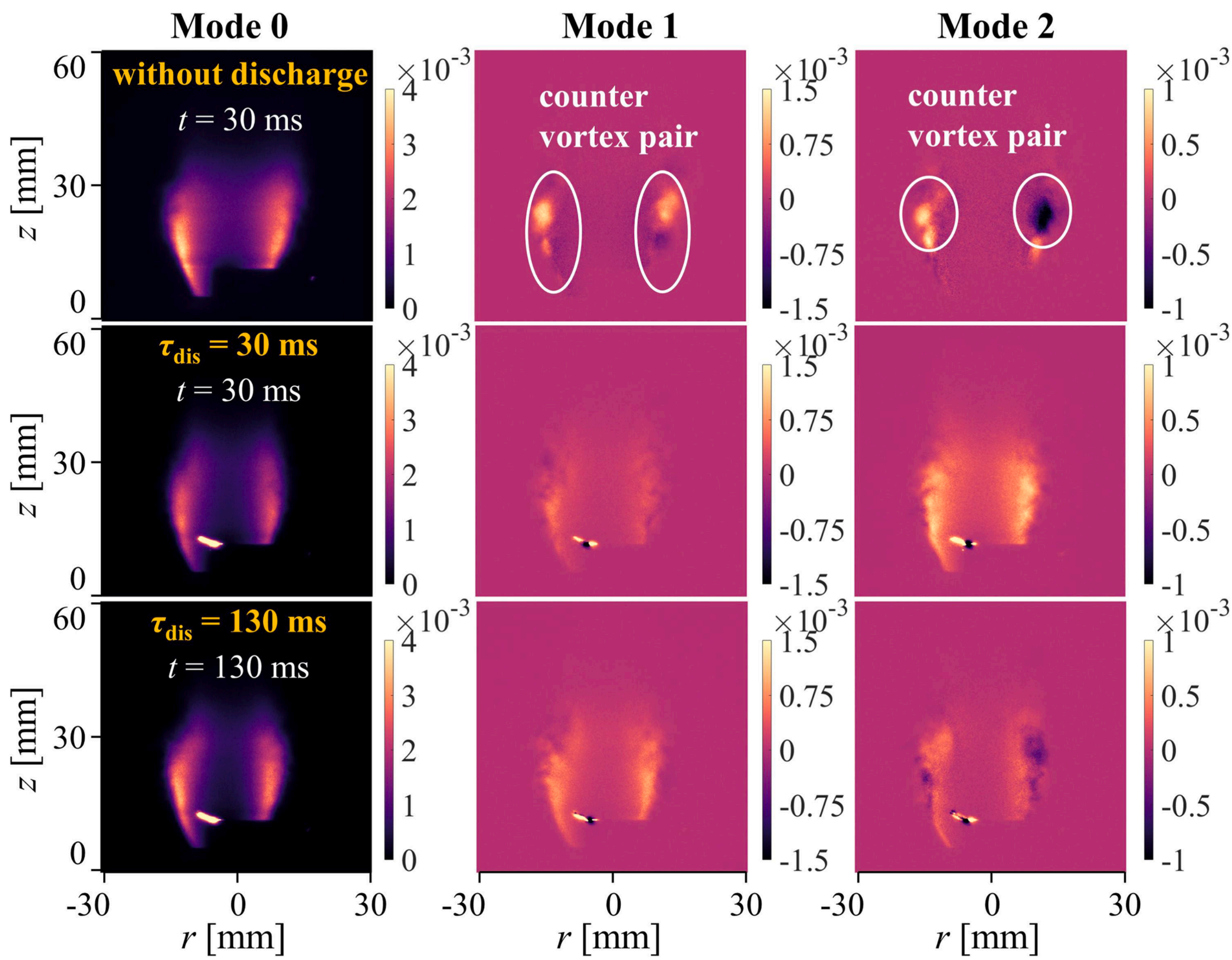

Fig. 9. The first 3 POD modes of perturbed flames without and with MRP discharges. (1) At t =130 ms without discharge (first row): λ_0, λ_1, and λ_2 = 0.78, 0.014, and 0.013; (2) at t =30 ms and τ_{dis} = 30 ms (second row): λ_0, λ_1, and λ_2 = 0.61, 0.10, and 0.09; (3) at t =130 ms and τ_{dis} = 130 ms (third row): λ_0, λ_1, and λ_2 = 0.65, 0.09, and 0.05.

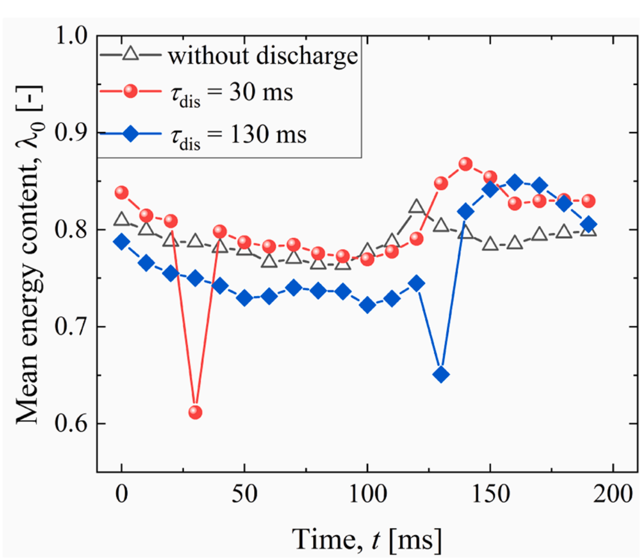

Fig. 10. Temporal variation of the mean energy content of perturbed flames.

130 ms, λ_0 decreases from 0.74 to 0.65 at t = 130 ms. In other words, the energy content of turbulent structures instantaneously increases by 0.20 and 0.09 at the instant of triggering the pulsed discharge. It means that the pulsed discharge causes a large disturbance to the flame, which is even more intense than the flow pulsation. The decrement in λ_0 can be attributed to the hydrodynamic effect of plasma-induced shockwave due to ultrafast heating of the pulsed discharge, which was reported to increase the wrinkling of the flame front and be responsible for the accelerated flame extinction [10,40,57]. However, the temporal decrement of λ_0 was not ever observed in some other studies. For example, λ_0 only exhibits an increasing trend when we previously applied a high-frequency gliding arc discharge [28] and when Rajasegar et al. applied a continuous microwave discharge [21] on similar premixed swirl flames. Therefore, the response of the mean energy distribution to different types of plasmas strongly depends on the plasma-altered flame dynamics.

3.5. Impacts of discharge repetition rate on LBO limits

For PSFs perturbed by positive fuel pulsations, the dependence of the LBO limit on the repetition rate (f) of the MRP discharge is shown in Fig. 11. Even at the maximum repetition rate of 200 Hz, the ratios of discharge power to thermal power under Q_{air} = 20, 30, and 40 L/min were quite low, 0.27%, 0.16%, and 0.10%, respectively. Here, the LBO limit exhibits a nonlinear trend versus the repetition rate. Taking the

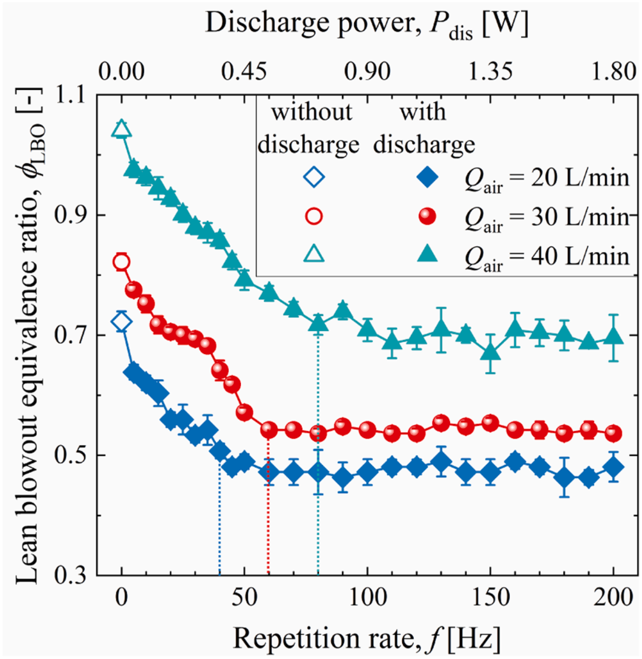

Fig. 11. LBO limits of perturbed PSFs versus the repetition rate of the MRP discharge. Dashed lines are added to mark the saturation repetition rates. The bottom and top axes denote the discharge repetition rate and the corresponding discharge power, respectively.

case of Q_{air} = 30 L/min as an example, the lean blowout equivalence ratio decreases from 0.82 to 0.54 as the repetition rate increases from 0 to 60 Hz, achieving a remarkable extension (34%) of the LBO limit. However, the LBO limit does not continue to decline when the repetition rate further increases. It could be interpreted from the perspective of the plasma-assisted reignition effect. Essentially, the MRP discharge with a higher repetition rate not only provides more radicals and heat, but also reignites the locally extinguished flame multiple times at various instants in one pulsating cycle. The "non-enhancement" regime will naturally merge into the "enhancement" regime. In addition, the pulse synergy of cumulative discharges may promote the inter-pulse coupling, increasing the ignition probability of the flame kernel [58]. Therefore, it shows better performance in extending LBO limits. In other words, as the repetition rate increases, the plasma-enhancement effect of MRP discharges can be extended to flames with higher flow rates. Actually, we have taken advantage of the high-frequency reignition of a 7.5 kHz gliding arc discharge to stabilize swirl flames with Reynolds numbers up to 10300 under air flow pulsations [28]. Nevertheless, when the flame is ultra-lean and even close to the flammability in reactive flows, multiple discharges in the local extinction zone cannot lead to successful reignition, resulting in a minimal ϕ_{LBO} and a corresponding saturation repetition rate [10]. Similar nonlinear enhancement from plasma was also observed in a prior study of Zhang et al. [59] which applied nanosecond pulsed discharge. It was reported that there is a saturation pulse number of 35-40 in reducing the ignition delay time of DME/O_2/Ar mixtures at an initial temperature of 800 K. Note that the energy per pulse of the present device is constant, so the plasma power increases with the repetition rate. At this point, the thermal and kinetic effects are enhanced simultaneously. However, if the average discharge power is kept constant, the effect of increasing the repetition rate might be different. Lacoste et al. [60] found that as the repetition rate of the nanosecond pulsed discharge increases, the thermal effect was strengthened but the kinetic effect was weakened, resulting in an overall flame response independent of the repetition rate. Hence, they concluded that the flame response is essentially determined by the coupled thermal and kinetic effects.

Moreover, the minimal ϕ_{LBO} of the plasma-assisted flame under fuel pulsation increases at a higher flow rate. For example, the minimal ϕ_{LBO} can be ultimately extended to 0.5 at Q_{air} = 20 L/min and 0.7 at Q_{air} = 40 L/min by plasma, corresponding to the saturation repetition rate of 40 Hz and 60 Hz, respectively. It suggests that when the MRP discharge assistance is saturated, the lean blowout is still strongly affected by the flow rate. In previous work by Rajasegar et el. using the powerful microwave plasma [22], the LBO limit extension was independent of the flow rate due to the change in flame dynamics from a lifted swirl flame to a plasma-stabilized flame anchored to the electrode. Whereas in the present work, the MRP discharge-assisted flame retains the typical pattern of a swirl-stabilized flame (see Fig. 7), the extended LBO limit is still influenced by the intrinsic PSF stability and thus dependent on the flow rate.

Furthermore, the relative importance of plasma-hydrodynamic effects produced by the repetitively pulsed discharge with different repetition rates can be estimated by a Strouhal number (St_d) of the discharge, defined as:

$$St_d = \frac{fd_c}{u_{in}} \tag{5}$$

where f is the forcing frequency of the plasma discharge and u_{in} is the inlet flow velocity. Essentially, the discharge Strouhal number is the ratio of the characteristic flow time (d_c/u_{in}) to the discharge period ($1/f$). Based on the saturation repetition rate (40, 60, and 80 Hz) at the three bulk flow velocities (1.6, 2.5, and 3.3 m/s), the values of St_d are estimated to be approximately 0.2. This consistency suggests that as the discharge frequency increase, the discharge period is decreased to a value comparable to the flow time, and the extension effect of pulsed discharge on the LBO limit saturates. It also interprets the underlying physics that a discharge with a sufficiently high repetition rate behaves like an igniter to process the pre-mixture. Optimal stabilization can be achieved when the interval between two discharges is enough short compared to the reactive flow.

4. Conclusion

This paper investigates the effects of the low-frequency fuel flow pulsation and the MRP discharge on the stability of the PSF. First, with the absence of the MRP discharge, both positive and negative fuel pulsations narrow the LBO limit by up to 46% compared to that without fuel pulsation. It can be largely attributed to the fluctuation of the local equivalence ratio during the periodic flame response to the pulsating disturbance. Moreover, the convective time delay between the fuel pulsation occurrence and the flame front is proposed to properly describe the flame evolution after a fuel flow pulsation.

Secondly, the effect of the MRP discharge on the LBO limit strongly depends on the discharge time delay. As the discharge is applied prior to the arrival of the equivalence ratio fluctuation (i.e., τ_{dis} = 0-90/160-200 ms), the flame suffering from the reduced equivalence ratio can be reignited and stabilized via thermal and kinetic enhancements. As a result, the LBO limit is extended by up to approximately 10%. Otherwise, the discharge contributes to less extension of the LBO limit. Furthermore, for the relatively complex flames where fuel pulsation and pulsed discharge coexist, we employed a quantitative post-processing technique of proper orthogonal decomposition on the OH-PLIF images. It reveals the two-sided effects of the MRP discharge on flame dynamics. On the one hand, the MRP discharge increases the mean energy content and suppresses flame turbulence, which ultimately improves flame stability even under fuel pulsation. On the other hand, the onset of the discharge arouses a kind of undesired plasma-induced hydrodynamics, which is too abrupt for a flame to stabilize.

Finally, the repetition rate of the MRP discharge is found to have a nonlinear impact on the LBO limit. Each flow rate corresponds to a saturation repetition rate. Taking the case of Q_{air} = 30 L/min as an example, the lean blowout equivalence ratio decreases with the repetition rate (< 60 Hz) and remains constant over 60 Hz. It can be attributed to the saturation of the plasma-induced reignition, which results from the thermal and kinetic effects. Additionally, these findings allow us to achieve efficient combustion assistance using single-channel discharge with minimal energy. Furthermore, we even find that at three different flow rates, the dimensionless discharge Strouhal number based on the saturation repetition rate is highly coincident with each other. It pronounces the importance of the discharge period compared to the characteristic flow time, and indicates that the domain of flame response to the repetitively pulsed discharge can be distinguished by the discharge frequency. In the low-frequency domain, the flame response is dependent on the frequency, whilst in the high-frequency domain, the plasma assistance reaches saturation.

Declaration of Competing Interest

The authors declare that they have no known competing financial interests or personal relationships that could have appeared to influence the work reported in this paper.

Data availability

Data will be made available on request.

Acknowledgments

This work was supported by the National Natural Science Foundation of China (Grants No. 51725601 and No. 91641204).

Supplementary materials

Supplementary material associated with this article can be found, in the online version, at doi:10.1016/j.jaecs.2023.100122.

References

[1] Shanbhogue SJ, Husain S, Lieuwen T. Lean blowoff of bluff body stabilized flames: Scaling and dynamics. Prog Energy Combust Sci 2009;35(1):98–120. https://doi.org/10.1016/j.pecs.2008.07.003.

[2] Dawson JR, Gordon RL, Kariuki J, Mastorakos E, Masri AR, Juddoo M. Visualization of blow-off events in bluff-body stabilized turbulent premixed flames. Proc Combust Inst 2011;33(1):1559–66. https://doi.org/10.1016/j.proci.2010.05.044.

[3] Chaudhuri S, Kostka S, Renfro MW, Cetegen BM. Blowoff dynamics of bluff body stabilized turbulent premixed flames. Combust Flame 2010;157(4):790–802. https://doi.org/10.1016/j.combustflame.2009.10.020.

[4] Kedia KS, Ghoniem AF. The blow-off mechanism of a bluff-body stabilized laminar premixed flame. Combust Flame 2015;162(4):1304–15. https://doi.org/10.1016/j.combustflame.2014.10.017.

[5] Sun Y, Sun M, Zhao D, Chen Y, Ma G, Wan M, et al. Blow-off characteristics of a premixed methane/air flame response to acoustic disturbances in a longitudinal combustor. Aerosp Sci Technol 2021;118:107003. https://doi.org/10.1016/j.ast.2021.107003.

[6] Tuttle SG, Chaudhuri S, Kopp-Vaughan KM, Jensen TR, Cetegen BM, Renfro MW, et al. Lean blowoff behavior of asymmetrically-fueled bluff body-stabilized flames. Combust Flame 2013;160(9):1677–92. https://doi.org/10.1016/j.combustflame.2013.03.009.

[7] Rosfjord TJ, Cohen JM. Evaluation of the transient operation of advanced gas-turbine combustors. J Propul Power 1995;11(3):497–504. https://doi.org/10.2514/3.23870.

[8] Kim KT, Lee JG, Quay BD, Santavicca D. Experimental investigation of the nonlinear response of swirl-stabilized flames to equivalence ratio oscillations. J Eng Gas Turbines Power 2010;133(2). https://doi.org/10.1115/1.4001999.

[9] Humphrey LJ, Emerson B, Lieuwen TC. Premixed turbulent flame speed in an oscillating disturbance field. J Fluid Mech 2018;835:102–30. https://doi.org/10.1017/jfm.2017.728.

[10] Cui W, Ren YH, Li SQ. Stabilization of premixed swirl flames under flow pulsations using microsecond pulsed plasmas. J Propul Power 2019;35(1):190–200. https://doi.org/10.2514/1.B37219.

[11] Sun J, Cui W, Tang Y, Kong C, Li S. Inlet pulsation-induced extinction and plasma-assisted stabilization of premixed swirl flames. Fuel 2022;328:125372. https://doi.org/10.1016/j.fuel.2022.125372.

[12] Muruganandam TM, Nair S, Scarborough D, Neumeier Y, Jagoda J, Lieuwen T, et al. Active control of lean blowout for turbine engine combustors. J Propul Power 2005;21(5):807–14. https://doi.org/10.2514/1.7254.

[13] Choi G-M, Tanahashi M, Miyauchi T. Control of oscillating combustion and noise based on local flame structure. Proc Combust Inst 2005;30(2):1807–14. https://doi.org/10.1016/j.proci.2004.08.249.

[14] Schefer RW. Hydrogen enrichment for improved lean flame stability. Int J Hydrogen Energy 2003;28(10):1131–41. https://doi.org/10.1016/S0360-3199(02)00199-4.

[15] Ju YG, Sun WT. Plasma assisted combustion: dynamics and chemistry. Prog Energy Combust Sci 2015;48:21–83. https://doi.org/10.1016/j.pecs.2014.12.002.

[16] Adamovich IV, Lempert WR. Challenges in understanding and predictive model development of plasma-assisted combustion. Plasma Phys Controlled Fusion 2014;57(1):014001. https://doi.org/10.1088/0741-3335/57/1/014001.

[17] Starikovskiy A, Aleksandrov N. Plasma-assisted ignition and combustion. Prog Energy Combust Sci 2013;39(1):61–110. https://doi.org/10.1016/j.pecs.2012.05.003.

[18] Takita K, Uemoto T, Sato T, Ju Y, Masuya G, Ohwaki K. Ignition characteristics of plasma torch for hydrogen jet in an airstream. J Propul Power 2000;16(2):227–33. https://doi.org/10.2514/2.5587.

[19] Tang Y, Zhuo JK, Cui W, Li SQ, Yao Q. Non-premixed flame dynamics excited by flow fluctuations generated from dielectric-barrier-discharge plasma. Combust Flame 2019;204:58–67. https://doi.org/10.1016/j.combustflame.2019.03.003.

[20] Ehn A, Petersson P, Zhu JJ, Li ZS, Alden M, Nilsson EJK, et al. Investigations of microwave stimulation of a turbulent low-swirl flame. Proc Combust Inst 2017;36(3):4121–8. https://doi.org/10.1016/j.proci.2016.06.164.

[21] Rajasegar R, Mitsingas CM, Mayhew EK, Yoo J, Lee T. Proper orthogonal decomposition for analysis of plasma-assisted premixed swirl-stabilized flame dynamics. IEEE Trans Plasma Sci 2016;44(12):2940–51. https://doi.org/10.1109/TPS.2016.2622687.

[22] Rajasegar R, Mitsingas CM, Mayhew EK, Hammack S, Do H, Lee T. Effects of continuous volumetric direct-coupled nonequilibrium atmospheric microwave plasma discharge on swirl-stabilized premixed flames. IEEE Trans Plasma Sci 2016;44(1):39–48. https://doi.org/10.1109/TPS.2015.2499754.

[23] Hwang J, Kim W, Bae C. Influence of plasma-assisted ignition on flame propagation and performance in a spark-ignition engine. Appl Energy Combust Sci 2021;6:100029. https://doi.org/10.1016/j.jaecs.2021.100029.

[24] Gao JL, Kong CD, Zhu JJ, Ehn A, Hurtig T, Tang Y, et al. Visualization of instantaneous structure and dynamics of large-scale turbulent flames stabilized by a gliding arc discharge. Proc Combust Inst 2019;37(4):5629–36. https://doi.org/10.1016/j.proci.2018.06.030.

[25] Kong C, Gao J, Zhu J, Ehn A, Aldén M, Li Z. Characteristics of a gliding arc discharge under the influence of a laminar premixed flame. IEEE Trans Plasma Sci 2019;47(1):403–9. https://doi.org/10.1109/TPS.2018.2877126.

[26] Lin B, Wu Y, Zhu Y, Song F, Bian D. Experimental investigation of gliding arc plasma fuel injector for ignition and extinction performance improvement. Appl Energy 2019;235:1017–26. https://doi.org/10.1016/j.apenergy.2018.11.026.

[27] Lee DH, Kim KT, Cha MS, Song YH. Optimization scheme of a rotating gliding arc reactor for partial oxidation of methane. Proc Combust Inst 2007;31(2):3343–51. https://doi.org/10.1016/j.proci.2006.07.230.

[28] Sun J, Tang Y, Li S. Plasma-assisted stabilization of premixed swirl flames by gliding arc discharges. Proc Combust Inst 2021;38(4):6733–41. https://doi.org/10.1016/j.proci.2020.06.223.

[29] Tang Y, Xie D, Shi B, Wang N, Li S. Flammability enhancement of swirling ammonia/air combustion using AC powered gliding arc discharges. Fuel 2022;313:122674. https://doi.org/10.1016/j.fuel.2021.122674.

[30] Sun J, Huang Q, Tang Y, Li S. Stabilization and emission characteristics of gliding arc-assisted NH3/CH4/air premixed flames in a swirl combustor. Energy Fuel 2022;36(15):8520–7. https://doi.org/10.1021/acs.energyfuels.2c01217.

[31] Tang Y, Sun J, Shi B, Li S, Yao Q. Extension of flammability and stability limits of swirling premixed flames by AC powered gliding arc discharges. Combust Flame 2021;231:111483. https://doi.org/10.1016/j.combustflame.2021.111483.

[32] Ju RY, Wang JH, Xia H, Li YM, Mu HB, Zhang GJ, et al. Effect of rotating gliding arc plasma on lean blow-off limit and flame structure of bluff body and swirl-stabilized premixed flames. IEEE Trans Plasma Sci 2021;49(11):3554–65. https://doi.org/10.1109/TPS.2021.3121286.

[33] Xiong Y, Schulz O, Bourquard C, Weilenmann M, Noiray N. Plasma enhanced auto-ignition in a sequential combustor. Proc Combust Inst 2019;37(4):5587–94. https://doi.org/10.1016/j.proci.2018.08.031.

[34] Shcherbanev S, Morinière T, Solana-Pérez R, Weilenmann M, Xiong Y, Doll U, et al. Anchoring of premixed jet flames in vitiated crossflow with pulsed nanosecond spark discharge. Appl Energy Combust Sci 2020;1-4:100010. https://doi.org/10.1016/j.jaecs.2020.100010.

[35] Chintala N, Meyer R, Hicks A, Bao A, Rich JW, Lempert WR, et al. Nonthermal ignition of premixed hydrocarbon-air flows by nonequilibrium radio frequency plasma. J Propul Power 2005;21(4):583–90. https://doi.org/10.2514/1.10865.

[36] Adamovich IV, Lempert WR, Nishihara M, Rich JW, Utkin YG. Repetitively pulsed nonequilibrium plasmas for magnetohydrodynamic flow control and plasma-assisted combustion. J Propul Power 2008;24(6):1198–215. https://doi.org/10.2514/1.24613.

[37] Mao X, Rousso A, Chen Q, Ju Y. Numerical modeling of ignition enhancement of CH4/O2/He mixtures using a hybrid repetitive nanosecond and DC discharge. Proc Combust Inst 2019;37(4):5545–52. https://doi.org/10.1016/j.proci.2018.05.106.

[38] Barbosa S, Pilla G, Lacoste DA, Scouflaire P, Ducruix S, Laux CO, et al. Influence of nanosecond repetitively pulsed discharges on the stability of a swirled propane/air

burner representative of an aeronautical combustor. Philos Trans A Math Phys Eng Sci 2015;373(2048):20140335. https://doi.org/10.1098/rsta.2014.0335.

[39] Sun W, Uddi M, Won SH, Ombrello T, Carter C, Ju Y. Kinetic effects of non-equilibrium plasma-assisted methane oxidation on diffusion flame extinction limits. Combust Flame 2012;159(1):221–9. https://doi.org/10.1016/j.combustflame.2011.07.008.

[40] Lacoste DA, Moeck JP, Durox D, Laux CO, Schuller T. Effect of nanosecond repetitively pulsed discharges on the dynamics of a swirl-stabilized lean premixed flame. J Eng Gas Turbines Power 2013;135(10). https://doi.org/10.1115/1.4024961.

[41] Moeck J, Lacoste D, Laux C, Paschereit C. Control of combustion dynamics in a swirl-stabilized combustor with nanosecond repetitively pulsed discharges. 51st AIAA Aerospace Sciences Meeting including the New Horizons Forum and Aerospace Exposition.

[42] Beer JM, Chigier NA. Combustion aerodynamics. Applied Science Publishers; 1974.

[43] Ducruix S, Durox D, Candel S. Theoretical and experimental determinations of the transfer function of a laminar premixed flame. Proc Combust Inst 2000;28(1):765–73. https://doi.org/10.1016/S0082-0784(00)80279-9.

[44] Zhang C, Shao T, Wang R, Huang W, Niu Z, Schamiloglu E. A repetitive microsecond pulse generator for atmospheric pressure plasma jets. IEEE Trns Dielectr Electr Insul 2015;22(4):1907–15. https://doi.org/10.1109/TDEI.2014.005042.

[45] Cuppoletti D, Ombrello T, Carter C, Hammack S, Lefkowitz J. Ignition dynamics of a pulse detonation igniter in a supersonic cavity flameholder. Combust Flame 2020;215:376–88. https://doi.org/10.1016/j.combustflame.2020.01.030.

[46] Lieuwen T, Zinn BT. The role of equivalence ratio oscillations in driving combustion instabilities in low NOx gas turbines. Proc Combust Inst 1998;27(2):1809–16. https://doi.org/10.1016/S0082-0784(98)80022-2.

[47] Hathout JP, Fleifil M, Annaswamy AM, Ghoniem AF. Combustion instability active control using periodic fuel injection. J Propul Power 2002;18(2):390–9. https://doi.org/10.2514/2.5947.

[48] Bernier D, Lacas F, Candel S. Instability mechanisms in a premixed prevaporized combustor. J Propul Power 2004;20(4):648–56. https://doi.org/10.2514/1.11461.

[49] Sun J, Ren Y, Tang Y, Li S. Influences of heat flux on extinction characteristics of steady/unsteady premixed stagnation flames. Proc Combust Inst 2021;38(2):2305–14. https://doi.org/10.1016/j.proci.2020.06.316.

[50] Kim W, Mungal MG, Cappelli MA. The role of in situ reforming in plasma enhanced ultra lean premixed methane/air flames. Combust Flame 2010;157(2):374–83. https://doi.org/10.1016/j.combustflame.2009.06.016.

[51] Choe J, Sun WT. Blowoff hysteresis, flame morphology and the effect of plasma in a swirling flow. J Phys D-Appl Phys 2018;51(36):365201. https://doi.org/10.1088/1361-6463/aad4dc.

[52] Qiu J, Zhang C, Han L, Ren C, Shao T. Characteristics of repetitive discharges of plasma synthetic jet actuators. In: 2016 IEEE International Power Modulator and High Voltage Conference (IPMHVC). IEEE; 2016. p. 576–9.

[53] Berkooz G, Holmes a P, Lumley JL. The proper orthogonal decomposition in the analysis of turbulent flows. Annu Rev Fluid Mech 1993;25(1):539–75. https://doi.org/10.1146/annurev.fl.25.010193.002543.

[54] Sirovich L. Turbulence and the dynamics of coherent structures. I. Coherent structures. Q Appl Math 1987;45(3):561–71. https://doi.org/10.1090/qam/910462.

[55] Chen H, Reuss DL, Hung DLS, Sick V. A practical guide for using proper orthogonal decomposition in engine research. Int J Engine Res 2012;14(4):307–19. https://doi.org/10.1177/1468087412455748.

[56] Fogleman M, Lumley J, Rempfer D, Haworth D. Application of the proper orthogonal decomposition to datasets of internal combustion engine flows. J Turbul 2004;5. https://doi.org/10.1088/1468-5248/5/1/023.

[57] Xu DA, Lacoste DA, Rusterholtz DL, Elias PQ, Stancu GD, Laux CO. Experimental study of the hydrodynamic expansion following a nanosecond repetitively pulsed dischage in air. Appl Phys Lett 2011;99(12). https://doi.org/10.1063/1.3641413.

[58] Dunn I, Ahmed KA, Leiweke RJ, Ombrello TM. Optimization of flame kernel ignition and evolution induced by modulated nanosecond-pulsed high-frequency discharge. Proc Combust Inst 2021;38(4):6541–50. https://doi.org/10.1016/j.proci.2020.06.104.

[59] Zhang Y, Yang S, Sun W, Yang V. Effects of non-equilibrium plasma discharge on ignition and NTC chemistry of DME/O2/Ar mixtures: a numerical investigation. In: 53rd AIAA/SAE/ASEE Joint Propulsion Conference; 2017.

[60] Lacoste DA, Xu DA, Moeck JP, Laux CO. Dynamic response of a weakly turbulent lean-premixed flame to nanosecond repetitively pulsed discharges. Proc Combust Inst 2013;34:3259–66. https://doi.org/10.1016/j.proci.2012.07.017.